

COSMOGLOBE DR1. III. First full-sky model of polarized synchrotron emission from all WMAP and Planck LFI data

D. Watts^{1*} and U. Fuskeland¹ et al.

Institute of Theoretical Astrophysics, University of Oslo, Blindern, Oslo, Norway

July 20, 2023

ABSTRACT

We present the first statistically consistent model of full-sky polarized synchrotron emission derived from the combination of all *WMAP* and *Planck* LFI frequency maps. The basis of this analysis are the end-to-end reprocessed COSMOGLOBE Data Release 1 sky maps presented in a companion paper, which have significantly lower instrumental systematics than the legacy products from each experiment. We find that the resulting polarized synchrotron amplitude map has an average noise rms of $2.4\mu\text{K}$ at 22 GHz and a smoothing scale of 2° FWHM, which is 30 % lower than the recently released BEYONDPLANCK model that included only LFI+*WMAP* *Ka-V* data, and it is 45 % lower than the raw *WMAP* *K*-band. The mean EE/BB power spectrum ratio is 0.27 ± 0.02 , which agrees well with previous estimates from both *Planck* and QUIJOTE. Assuming a power law model for the synchrotron spectral energy density, we find a full-sky inverse noise-variance weighted mean of $\beta_s = -3.06 \pm 0.08$ between *WMAP* *K*-band and LFI 30 GHz, in good agreement with previous estimates. At high Galactic latitudes, however, we find $\beta_s = -3.31 \pm 0.08$, which is slightly steeper than most previous foregrounds-oriented estimates, but in good agreement with the *Planck* 2018 LFI CMB likelihood result of $\beta_s = -3.27 \pm 0.04$. For comparison, the corresponding full-sky and high-latitude estimates derived from the official *WMAP* and LFI products are $\beta_s = -3.44 \pm 0.08$ and $\beta_s = -3.71 \pm 0.08$, respectively. These values are obviously compromised by large-scale instrumental systematics in both *WMAP* and LFI. In summary, the novel COSMOGLOBE DR1 synchrotron model is both more sensitive and systematically cleaner than similar previous models, and it has a more complete error description that is defined by a set of Monte Carlo posterior samples. We believe that these products are preferable for all synchrotron-related scientific applications, including simulation, forecasting and component separation.

Key words. ISM: general – Cosmology: observations, polarization, cosmic microwave background, diffuse radiation – Galaxy: general

Contents

1	Introduction
2	Data products
2.1	WMAP and Planck legacy data products
2.2	The Cosmoglobe data products
3	TT-plot method
4	Maximum likelihood estimation
5	Angular power spectra
6	Discussion and conclusion

1. Introduction

Understanding the polarization of the cosmic microwave background (CMB) is a primary focus of observational cosmology in the coming decades. Following the success of the satellite-based COBE, *WMAP*, and *Planck* experiments, as well as the sub-orbital experiments including, e.g., BICEP, ACT, SPT, Polarbear, and many others, the future LiteBIRD satellite and ground-based Simons Observatory (SO) and CMB-S4 experiments will create

the most sensitive maps of the polarized sky yet, providing the most stringent constraints on primordial gravitational waves.

- 1** In the past decade, uncertainty on cosmological constraints has been limited not only by instrumental sensitivity, but by incomplete knowledge of the sky itself. These analysis difficulties have been mitigated by analyzing maps from different experiments, e.g., [BICEP2/Keck Array and Planck Collaborations \(2015\)](#), or designing of experiments with broad frequency coverage, such as *WMAP* ([Bennett et al. 2013](#)) and *Planck* [Collaboration I \(2020\)](#). A major impediment to joint analyses is the difficulty of combining data with different survey strategies and incompletely characterized systematics. In order to maximize scientific throughput, one must either design an experiment that can characterize every relevant observable on its own, or jointly analyze different datasets in the same joint framework.

The BEYONDPLANCK project achieved this joint analysis by combining external data, i.e., the Haslam 408 MHz map ([Haslam et al. 1982](#)), *WMAP* *Ka-V* bands, *Planck* 353 GHz in polarization, and *Planck* 857 GHz in intensity, while analyzing the *Planck* 30, 44, and 70 GHz TOD ([BeyondPlanck Collaboration 2023](#)). The *Planck* LFI experiment showed that raw detector sensitivity was not enough to obtain high-fidelity sky maps; [Planck Collaboration II \(2020\)](#) found that the detector gain solution depended on the assumed polarization and intensity of the sky. To break this circular dependency, the BEYONDPLANCK framework solved for the intrinsic sky signal and instrumental parameters iteratively, providing an accurate model of the entire

* Corresponding author: D. Watts; duncanwa@astro.uio.no

system with full error propagation. By leveraging external data, BEYONDPLANCK was able to create *Planck* LFI of cosmological quality, while generating a robust model of the foreground sky.

In COSMOGLOBE DR1 (Watts et al. 2023), this end-to-end framework was extended, performing a joint analysis of the same data as BEYONDPLANCK while adding the full *WMAP* time-ordered data. This analysis not only improved the quality of the *WMAP* maps themselves, but provided the most robust full-sky model of low frequency polarized emission available to date.

In order to make use of the synchrotron model, we require robust estimates of the spectral behavior. Fundamental behaviors, such as the spectral index as a function of frequency, spatial decorrelation, and even the functional form of the SED, are yet to be fully characterized observationally. Modern attempts have been stymied by the lack of high signal-to-noise data; de Beslunce et al. (2022), for example, find spectral indices ranging from -5 to -1 , well outside of the theoretical limits of (?), given in, e.g., (?). This discrepancy is largely due to inadequate data coverage, requiring higher signal-to-noise datasets that have not yet been generated. Therefore, any conclusions about the distribution of the polarized synchrotron spectral index must be verified through multiple independent analysis methods and data choices.

In this work, we will use the *WMAP* and LFI maps generated in the COSMOGLOBE DR1 analysis. We perform three separate analyses; a linear correlation within regions (T-T plots), angular power spectra, and per-pixel Gibbs sampling.

For the power spectra, compare with, e.g., Figure 33 of Planck Collaboration IV (2018). We use the same bins as in Table C.1 of Planck Collaboration XI (2020)

2. Data products

In this paper, we investigate the spatial variation of the polarized synchrotron spectral index, with an emphasis on the comparison between legacy maps against the COSMOGLOBE results. The data products used are the *WMAP* and *Planck* LFI maps, with most of the statistical weight coming from 23–33 GHz. These frequencies are low enough that we can treat them as synchrotron tracers and hence ignore thermal dust and CMB, but not so low as we need to take into account effects like Faraday rotation (Fuske-land et al. 2021). The legacy data products and the data products from the COSMOGLOBE *WMAP* reanalysis (Watts et al. 2023), are described in the two following sections.

2.1. WMAP and Planck legacy data products

The Wilkinson Microwave Anisotropy Probe (Bennett et al. 2013, *WMAP*) was a NASA-funded satellite mission that observed from August 2001 to August 2010, designed to characterize the microwave sky well enough to measure the primary CMB anisotropies across the full sky down to a resolution of $13'$. Using a differential scanning strategy inspired by *COBE/DMR*, *WMAP* produced maps of the sky at 23 (*K*), 33 (*Ka*), 41 (*Q*), 61 (*V*), and 94 GHz (*W*) in both polarization and intensity (Bennett et al. 2013), with angular resolutions of $53'$ at 23 GHz to $13'$ at 94 GHz. The maps are available on the LAMBDA website.¹

The *Planck* Low Frequency Instrument (LFI) produced 30, 44, and 70 GHz maps in both intensity and polarization, while the High Frequency Instrument (HFI) produced 100, 143, 217, 353 GHz maps in polarization and intensity, and 545 and

857 GHz maps in intensity alone. The LFI data in particular are similar to the *WMAP* data, with higher angular resolutions of $30'$, $20'$, and $13'$ for 30, 44, and 70 GHz, and with higher sensitivity. Although the detector design was similar, LFI observed with a single horn, and observed in rings closely aligned with the ecliptic longitude. The legacy datasets, PR3 (Planck Collaboration I 2020) and PR4 (Planck Collaboration Int. LVII 2020), are both publicly available on the *Planck* Legacy Archive (PLA).²

2.2. The Cosmoglobe data products

The goal of COSMOGLOBE is to perform joint end-to-end analyses on several data sets jointly, preferably beginning from raw time-ordered data (TOD). Doing this can help to break the degeneracies of the different data sets, and in general reduced the amplitude of systematic effects. The analysis performed in BeyondPlanck Collaboration (2023) and Watts et al. (2023) was performed on raw TOD to cosmological parameters using the Bayesian Gibbs sampler, Commander3. The data products produced in these analysis account for the complex interactions between the instrument, the microwave sky, and its consistent components self-consistently.

The analysis in this paper makes use of COSMOGLOBE end products produced by the reanalysis of the *WMAP* and *Planck* LFI TODs (Watts et al. 2023). This analysis produced improved *WMAP* and *Planck* LFI maps, which we will use in an analysis to compare to the legacy data. In particular, we are interested in exactly the same set of maps as in the previous section in order to be able to do a comparison study. The pixelization and angular scale are the same as for the legacy products ($N_{\text{side}} = 64$, 1° FWHM). The COSMOGLOBE end products consists of a series of 500 samples from the Gibbs chain, instead of just one mean sample as has been the normal case for previous data releases.

While the COSMOGLOBE pipeline produces samples of polarized synchrotron emission, the spatial variation of the spectral index is poorly determined within the Gibbs chain. To mitigate the poor MCMC convergence of the spectral indices, the COSMOGLOBE DR1 sampled the spectral index from a prior distribution, $\beta_s \sim N(-3.15, 0.05^2)$. Improvements within the Commander3 framework will require more high signal-to-noise data and algorithmic improvements within the codebase.

The polarized spectral amplitude determined from COSMOGLOBE compares favorably to previous estimates using *WMAP* and *Planck* LFI data, as shown in Fig. 1. We plot the total polarized amplitude $P = \sqrt{Q^2 + U^2}$ for ease of comparison, although it creates a visible noise bias in the low amplitude regions. Each of these maps were produced with slightly different pipelines and datasets. The top row shows *Planck* PR4 and *WMAP*9, and consists of entirely different datasets.³ The synchrotron solution is driven by the lowest frequency map, 30 GHz and *K*-band respectively, so any difference in the amplitude maps are due to differences in a combination of data processing, instrumental properties, and the microwave sky at 23 GHz and 30 GHz.

The synchrotron amplitude maps from end-to-end processing, BEYONDPLANCK and COSMOGLOBE, contain slightly different datasets, but sample the instrumental properties and sky properties jointly. Of these maps, BEYONDPLANCK has lower resolution and higher noise, in large part because COSMOGLOBE is able to use the reprocessed *WMAP* *K*-band map.

² <https://pla.esac.esa.int/>

³ Perhaps several samples of *WMAP*-only would be useful to compare apples-to-apples, since these are all Commander3 products.

¹ https://lambda.gsfc.nasa.gov/product/wmap/dr5/m_products.html



Fig. 1. Improvement of synchrotron polarization amplitude $P = \sqrt{Q^2 + U^2}$.



Fig. 2. (Top:) Posterior standard deviation of COSMOGLOBE synchrotron polarization amplitude maps. (Bottom:) COSMOGLOBE posterior standard deviation divided by BEYONDPLANCK posterior standard deviation. The ratio is less than one for all pixels.

The COSMOGLOBE synchrotron map has a mean posterior rms of $2.4 \mu\text{K}$, a marked improvement over the BEYONDPLANCK map, as shown in Fig. 2. The rms map itself contains high signal-to-noise regions corresponding to the WMAP circles about the

ecliptic poles as well as the *Planck* rings and multiple ecliptic polar crossings. The main clear astrophysical variation comes in the forms of a thin region about the Galactic plane and several low-latitude point sources. Much of the improvement can be seen more clearly when taking the ratio of the posterior rms's, as in the bottom panel of Fig. 2. As expected, the regions with the lowest ratios correspond to the deep WMAP observations and the Galactic plane, which benefit from the high signal-to-noise of the K -band data. Regions with nearly identical rms include regions with the highest *Planck* depth, i.e., the ecliptic poles, and regions less deeply observed by WMAP, corresponding to planet crossings and artifacts from the processing mask. Notably, stripes corresponding the *Planck* scan strategy also show improvement respect to BEYONDPLANCK. This is due to the interaction between the sky model and LFI's instrumental parameters – with the high signal-to-noise K -band data, the sky model becomes more stable, and LFI's relative gain solution becomes better determined.

3. TT-plot method

Following Fuskeland et al. (2014) and Fuskeland et al. (2021), we apply linear regression via the T-T (“temperature-temperature”) method, in which spectral indices can be estimated over extended regions with approximately constant spectral indices. In this approach, our data model for two frequencies is

$$\mathbf{m}_\nu = \mathbf{m}_{\nu_0} \left(\frac{\nu}{\nu_0} \right)^\beta + o_\nu + \mathbf{n}_\nu, \quad (1)$$

where \mathbf{m}_ν is a spatially varying amplitude map, ν_0 is the reference frequency, β the power law between the two frequencies, o_ν the spatially constant offset per band, and \mathbf{n}_ν the noise. In the case of noiseless data with no offset, the spectral index may be



Fig. 3. The sky is split into the same 24 regions as in Fuskeland et al. (2014). The most prominent point sources are masked out and shown as the grey circular areas.

estimated using a simple ratio,

$$\frac{m_{\nu_1,p}}{m_{\nu_2,p}} = \left(\frac{\nu_1}{\nu_2} \right)^{\beta_{s,p}} \Rightarrow \beta_{s,p} = \frac{\ln(m_{\nu_1,p}/m_{\nu_2,p})}{\ln(\nu_1/\nu_2)} \quad (2)$$

The standard T-T plot method performs a linear regression $\mathbf{m}_{\nu_1} = a\mathbf{m}_{\nu_2} + b$, and associates β_s with $\ln a / \ln(\nu_1/\nu_2)$. More care must be taken when the noise amplitudes in both maps are comparable, so we adopt the effective variance method of Orear (1982) as implemented by Fuskeland et al. (2014).

For the T-T plot analysis, we focus exclusively on bands between 23 and 33 GHz. As in Fuskeland et al. (2014), we use the *WMAP* K and Ka band Stokes Q and U parameter maps at 23 GHz and 33 GHz. The respective effective frequencies used are 22.45 GHz and 32.64 GHz. The maps originally at a HealPix pixelization of $N_{\text{side}} = 512$ are downgraded to $N_{\text{side}} = 64$ and smoothed to a common resolution of 1° FWHM. The *Planck* data products used are the Ka band Stokes Q and U maps at 30 GHz. We use an effective frequency of 28.4 GHz. The products are natively at $N_{\text{side}} = 1024$, but as for the *WMAP* products, the maps are downgraded to $N_{\text{side}} = 64$ and smoothed to 1° FWHM.

Much better propagation of uncertainties with a whole suite of maps.

The uncertainty is calculated as the minimum of the uncertainties in each rotation angle, and region. As in the Fuskeland 2021 paper, an systematic uncertainty that takes into account the variation of beta over rotation angle; $[\max(\beta_\alpha) - \min(\beta_\alpha)]/2$ is added in quadrature to the statistical uncertainty. For the Cosmoglobe analyses the standard deviation of the spectral indices for all samples is also added in quadrature to represent an additional systematic uncertainty.

We will also use Table 6, Figure (33) of Planck 2018 results IV Diffuse component separation

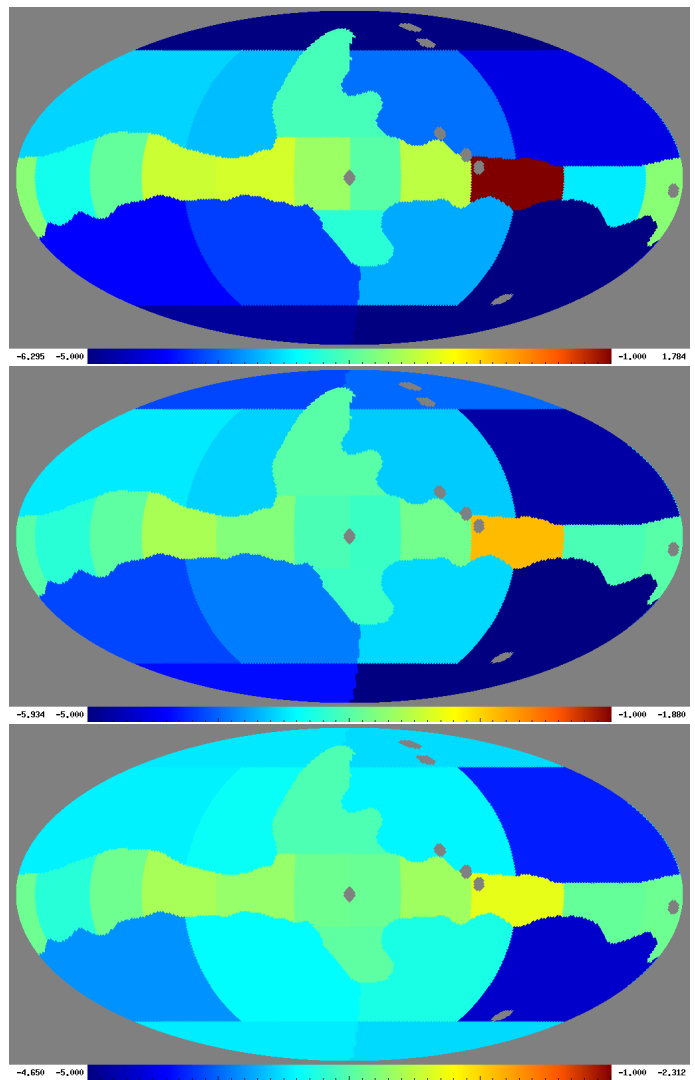


Fig. 4. The spatial variation of the synchrotron spectral index, computed using T-T plot between the *WMAP* 23 GHz and *Planck* 2018 30 GHz (top), *WMAP* 23 GHz and *Planck* DR4 30 GHz (middle) and Cosmoglobe 23 GHz and Cosmoglobe 30 GHz (bottom). The spectral index is inverse variance weighted over rotation angle, and in the Cosmoglobe case also samples. Fix style of maps. Bottom figure will be updated using more samples.

- Haslam, C. G. T., Salter, C. J., Stoffel, H., & Wilson, W. E. 1982, A&AS, 47, 1
 Orear, J. 1982, American Journal of Physics, 50, 912
 Planck Collaboration I. 2020, A&A, 641, A1
 Planck Collaboration II. 2020, A&A, 641, A2
 Planck Collaboration IV. 2018, A&A, 641, A4
 Planck Collaboration XI. 2020, A&A, 641, A11
 Planck Collaboration Int. LVII. 2020, A&A, 643, A42
 Watts, D. J. et al. 2023 [arXiv:2303.08095]

4. Maximum likelihood estimation

5. Angular power spectra

6. Discussion and conclusion

References

- Bennett, C. L., Larson, D., Weiland, J. L., et al. 2013, ApJS, 208, 20
 BeyondPlanck Collaboration. 2023, A&A, 675, A1
 BICEP2/Keck Array and Planck Collaborations. 2015, Phys. Rev. Lett., 114, 101301
 de Belsunce, R., Gratton, S., & Efstathiou, G. 2022, MNRAS, 517, 2855
 Fuskeland, U., Andersen, K. J., Aulien, R., et al. 2021, A&A, 646, A69
 Fuskeland, U., Wehus, I. K., Eriksen, H. K., & Næss, S. K. 2014, ApJ, 790, 104



Fig. 5. The synchrotron spectral index as a function of region number, computed using T-T plot between the 9-yr *WMAP* 23 GHz and *Planck* 2018 30 GHz (red), 9-yr *WMAP* 23 GHz and *Planck* DR4 30 GHz (blue) and Cosmoglobe 23 GHz and Cosmoglobe 30 GHz (black). The spectral index is inverse variance weighted over rotation angles, and samples. The horizontal line in the high latitude regions corresponds to the estimated spectral index values from the *Planck* 2018 likelihood analysis. [cite??](#) Figure will be updated using more samples.



Fig. 6. The synchrotron spectral index computed using T-T plot with the Cosmoglobe 23 GHz and 30 GHz data versus Cosmoglobe 23 GHz and 33 GHz data for the 24 regions. [Figure will be updated using more samples.](#)



Fig. 7. T-T plots for Stokes Q and U maps of the Cosmoglobe 23 GHz versus the Cosmoglobe 30 GHz (black) and the 9 yr WMAP 23 GHz versus Planck 2018 30 GHz (red) for all regions. The horizontal (solid and dotted) lines indicates the corresponding inverse variance weighted values of the spectral index, averaged over rotation angle. **Figure will be updated using more samples.**



Fig. 8. The synchrotron spectral index as a function of rotation angle, computed using T-T plot between the Cosmoglobe 23 GHz and the Cosmoglobe 30 GHz (black) compared to the spectral index using the 9 yr *WMAP* 23 GHz and *Planck* 2018 30 GHz (red) for all regions. The horizontal (solid and dotted) lines indicates the corresponding inverse variance weighted values of the spectral index. **Figure will be updated using more samples.**



Fig. 9. The spatial variation of the synchrotron spectral index, computed using T-T plot between the Cosmoglobe WMAP K band and Ka band. The spectral index is inverse variance weighted over rotation angle, and samples. Fix style of maps. Figure will be updated using more samples.



Fig. 10. The uncertainty of the synchrotron spectral index, computed using T-T plot between the Cosmoglobe WMAP K band and Ka band. REMOVE? Figure will be updated using more samples.



Fig. 11. The synchrotron spectral index, computed using T-T plot between the Cosmoglobe WMAP K band and Ka band (red) compared to the spectral index using the original 9 yr WMAP data (black) as a function of region number. The spectral index is inverse variance weighted over rotation angles, and samples. Figure will be updated, adding larger final uncertainty and using more samples.



Fig. 12. The synchrotron spectral index as a function of rotation angle, computed using T-T plot between the Cosmoglobe WMAP K band and Ka band (red) compared to the spectral index using the original 9 yr WMAP data (black) for all regions. The horizontal lines indicates the corresponding inverse variance weighted values of the spectral index. **Figure will be updated using more samples.**